



**HAL**  
open science

## Impact of electronic correlations on the equation of state and transport in $\epsilon$ -Fe

L. V. Pourovskii, J. Mravlje, M. Ferrero, Olivier Parcollet, I. A. Abrikosov

► **To cite this version:**

L. V. Pourovskii, J. Mravlje, M. Ferrero, Olivier Parcollet, I. A. Abrikosov. Impact of electronic correlations on the equation of state and transport in  $\epsilon$ -Fe. *Physical Review B*, 2014, 90 (15), pp.155120. 10.1103/PhysRevB.90.155120 . cea-01232842

**HAL Id: cea-01232842**

**<https://cea.hal.science/cea-01232842>**

Submitted on 24 Nov 2015

**HAL** is a multi-disciplinary open access archive for the deposit and dissemination of scientific research documents, whether they are published or not. The documents may come from teaching and research institutions in France or abroad, or from public or private research centers.

L'archive ouverte pluridisciplinaire **HAL**, est destinée au dépôt et à la diffusion de documents scientifiques de niveau recherche, publiés ou non, émanant des établissements d'enseignement et de recherche français ou étrangers, des laboratoires publics ou privés.

# Impact of electronic correlations on the equation of state and transport in $\epsilon$ -Fe

L. V. Pourovskii,<sup>1,2</sup> J. Mravlje,<sup>3</sup> M. Ferrero,<sup>1</sup> O. Parcollet,<sup>4</sup> and I. A. Abrikosov<sup>5</sup>

<sup>1</sup>*Centre de Physique Théorique, CNRS, École Polytechnique, 91128 Palaiseau, France*

<sup>2</sup>*Swedish e-science Research Centre (SeRC), Department of Physics, Chemistry and Biology (IFM), Linköping University, Linköping, Sweden*

<sup>3</sup>*Josef Stefan Institute, SI-1000, Ljubljana, Slovenija*

<sup>4</sup>*Institut de Physique Théorique (IPhT), CEA, CNRS, URA 2306, F-91191 Gif-sur-Yvette, France*

<sup>5</sup>*Department of Physics, Chemistry and Biology (IFM), Linköping University, Linköping, Sweden*

We have obtained the equilibrium volumes, bulk moduli, equations of state of the ferromagnetic cubic  $\alpha$  and paramagnetic hexagonal  $\epsilon$  phases of iron in close agreement with experiment using an *ab initio* dynamical mean-field theory approach. The local dynamical correlations are shown to be crucial for a successful description of the ground-state properties of paramagnetic  $\epsilon$ -Fe. Moreover, they enhance the effective mass of the quasiparticles and reduce their lifetimes across the  $\alpha \rightarrow \epsilon$  transition leading to a step-wise increase of the resistivity, as observed in experiment. The calculated magnitude of the jump is significantly underestimated, which points to non-local correlations. The implications of our results for the superconductivity and non-Fermi-liquid behavior of  $\epsilon$ -Fe are discussed.

PACS numbers:

Understanding properly pressurized iron is important for the geophysics of the inner Earth core [1] as well as for technological applications of this metal. In the range 12-16 GPa [2, 3] a martensitic transition from the body-centered-cubic (bcc) ferromagnetic phase ( $\alpha$ -Fe) to the hexagonal close-packed (hcp) phase ( $\epsilon$ -Fe) takes place. This  $\epsilon$ -Fe phase, discovered in 1956, [4] exhibits surprising magnetic and electronic properties, including superconductivity in the range of pressures from 13 to 31 GPa with a maximum transition temperature of about 2 K[5] as well as a non-Fermi-liquid normal state observed in the same pressure range [6].

Perhaps the most puzzling aspect of  $\epsilon$ -Fe is its magnetism, or rather an unexpected absence of it. Indeed, density-functional-theory (DFT) *ab initio* calculations within the generalized-gradient approximation (GGA) predict an antiferromagnetic ground state for the  $\epsilon$  phase, with either collinear [7–9] or non-collinear [10] order, which has up to date eluded experimental detection. While an anomalous Raman splitting observed in  $\epsilon$ -Fe [11] has been related to a possible antiferromagnetic order [12], no magnetic splitting has been detected in this phase by Mössbauer spectroscopy down to temperatures of several Kelvins [13, 14]. A collapse of the ordered magnetism across the  $\alpha - \epsilon$  transition has also been observed in the x-ray magnetic circular dichroism and in the x-ray absorption spectroscopy measurements [2]. A spin-fluctuation pairing mechanism that has been proposed for the superconducting phase [15] seems as well incompatible with the large-moment antiferromagnetism. If the non-magnetic ground state is imposed, the DFT-GGA total energy calculations predict an equation of state that drastically disagrees with experiment. The bulk modulus is overestimated by more than 50% and the equilibrium volume is underestimated by 10% compared to the experimental values [7]. Therefore, the ground state properties

of the observed non-magnetic  $\epsilon$ -Fe remain theoretically unexplained.

Another puzzling experimental observation is a large enhancement in the resistivity across the  $\alpha$ - $\epsilon$  transition, with the room temperature total resistivity of  $\epsilon$ -Fe being twice as large as that of the  $\alpha$  phase [16]. The electron-phonon-scattering contribution to resistivity calculated within GGA is in excellent agreement with the experimental total resistivity for the  $\alpha$  phase [17], however, these calculations predict virtually no change in the resistivity across the transition to antiferromagnetic hcp-Fe. The enhancement of resistivity in  $\epsilon$ -Fe seems likely to be caused by the ferromagnetic spin-fluctuations as the resistivity  $\rho$  follows  $\rho \propto T^{5/3}$  [6, 18]. This again is at odds with the antiferromagnetism suggested by the GGA calculations.

All this points to the possible importance of the electronic correlations that are not correctly incorporated in the local or semi-local DFT. In this paper, we show that including local dynamical many-body effects significantly improves the description of iron. Within a local-density-approximation+dynamical mean-field theory (LDA+DMFT) framework we obtain the ground state properties and the equation of states (EOS) of both ferromagnetic  $\alpha$  and paramagnetic  $\epsilon$  phases of iron as well as the  $\alpha$ - $\epsilon$  transition pressure and volume change in good agreement with experiment. The strength of the electronic correlations is significantly enhanced at the  $\alpha \rightarrow \epsilon$  transition. This leads to a reduced binding, which explains the relatively low value of the measured bulk modulus in  $\epsilon$ -Fe. The calculated resistivity has a jump at the transition but the magnitude of the jump is severely underestimated compared with the experimental value, which points to additional scattering not present in our local approach.

Previously, the local correlations have been found to

improve the description of the high-temperature paramagnetic  $\alpha$ -Fe [19, 20]. Moreover, the recently discovered electronic topological transition in  $\epsilon$ -Fe has been successfully explained by LDA+DMFT but not captured within LDA and GGA [21]. However, no attempts to study ground state and transport properties of  $\epsilon$ -Fe within an LDA+DMFT approach has been reported up to date.

We have employed a fully self-consistent method [22, 23] combining a full-potential band structure technique [24] and LDA for the exchange/correlations with the dynamical mean-field theory (DMFT) [25] treatment of the onsite Coulomb repulsion between Fe  $3d$  states. The Wannier orbitals representing Fe  $3d$  states were constructed from the Kohn-Sham states within the energy range from -6.8 to 5.5 eV. The DMFT quantum impurity problem was solved with the numerically exact hybridization-expansion continuous-time quantum Monte-Carlo (CT-QMC) method [26] using an implementation based on the TRIQS libraries [27] package. The local Coulomb interaction in the spherically-symmetric form was parametrized by the Slater integral  $F_0 = U = 4.3$  eV and Hund's rule coupling  $J = 1.0$  eV chosen to reproduce the value of the ordered magnetic moment in  $\alpha$ -Fe of  $2.2 \mu_B$  at its experimental volume. These values are somewhat larger than  $F_0 = U = 3.4$  eV and  $J = 0.9$  eV obtained by a constrained-random-phase-approximation (cRPA) method in Ref. [28] for  $\alpha$ -Fe. The 30% increase with respect to the static cRPA values accounts for the frequency dependence of the Coulomb vertex [29]. We used the around-mean-field form of the double counting correction [30] in this work. We verified that the lowest-energy collinear anti-ferromagnetic order "AFM-II" [7] collapses at the largest experimental volume of  $\epsilon$ -Fe in LDA+DMFT-CTQMC calculations with a rotationally-invariant local Coulomb repulsion [31]. However, non-density-density terms in the Coulomb vertex increase dramatically the computational cost of CT-QMC and preclude reaching the high accuracy required to extract an equation of state. Hence, we adopted the paramagnetic phase for  $\epsilon$ -Fe and employed the density-density approximation for the local Coulomb interaction throughout. This allowed us to use the fast "segment picture" algorithm of the CT-QMC [26] reaching an accuracy of about 0.1 meV/atom in the total energy computed in accordance with Ref. [23]. All our calculations were done for a relatively low temperature  $T = 290$  K. Thus the phonon and entropic contributions were neglected in the phase stability calculations. The conductivity in DMFT is  $\rho^{-1} = 2\pi e^2 \hbar \int d\omega \sum_k -(\partial f / \partial \omega) v_k A_k(\omega) v_k A_k(\omega)$  with implicit summation over band indices [32]. We calculated the band velocities  $v_k$  using the Wien2k optics package [24, 33] and we constructed the spectral functions  $A_k(\omega)$  from the highly precise DMFT self-energies (computed using  $10^{11}$  CT-QMC moves) which we analytically continued to the real axis using Padé approximants.

The obtained LDA+DMFT total energies vs. volume

TABLE I: Equilibrium atomic volume  $V$  (a.u.<sup>3</sup>/atom) and bulk modulus  $B$  (GPa) of bcc and hcp Fe computed by different *ab initio* approaches. The *FM*, *PM*, and *NM* subscripts indicate ferromagnetic, paramagnetic, non-magnetic state, respectively, *AFM-II* is the lowest energy collinear magnetic structure of  $\epsilon$ -Fe in accordance with GGA calculations of Ref. [7].

<b>bcc</b>	LDA+DMFT <sub>FM</sub>	GGA <sub>FM</sub>	expt. <sub>FM</sub>	
V	78.4	76.5 <sup>a</sup> , 77.2 <sup>b</sup> , 77.9 <sup>c</sup>	78.9	
B	168	187 <sup>a</sup> , 174 <sup>b</sup> , 186 <sup>c</sup>	172	
<b>hcp</b>	LDA+DMFT <sub>PM</sub>	GGA <sub>NM</sub>	GGA <sub>AFM-II</sub>	expt.
V	73.4	68.9 <sup>a</sup> , 69 <sup>d</sup>	71.2 <sup>d</sup>	75.4 <sup>e</sup>
B	191	288 <sup>a</sup> , 292 <sup>d</sup>	209 <sup>d</sup>	165 <sup>e</sup>

LDA+DMFT values are from this work. GGA and exp. values are from a). this work b). [34], c). [9], d). [7], e). [35]

in the  $\alpha$  and  $\epsilon$  phases are plotted in Fig 1a. Our calculations predict the ferromagnetic bcc  $\alpha$  phase to be the ground state. The transition to a paramagnetic  $\epsilon$ -Fe (the common tangent shown in Fig 1a) is predicted to occur at a pressure  $P_c$  of 10 GPa. The paramagnetic  $\alpha$  phase is about 10 mRy or 1500 K higher in energy, in good correspondence to the Curie temperature of  $\alpha$ -Fe. In Table I we list the resulting LDA+DMFT equilibrium atomic volumes and bulk moduli obtained by the fitting of calculated energy-volume data with Birch-Murnaghan EOS [36]. Also shown are GGA lattice parameters and bulk moduli obtained by us and in previous works, as well as corresponding experimental values. The LDA+DMFT dramatically improves agreement with the experiment for paramagnetic  $\epsilon$ -Fe for both the volume and bulk modulus, thus correcting the large overbinding error of GGA. The paramagnetic LDA+DMFT results are still closer to experimental values than the AFM GGA ones. Hence, even by adopting a magnetic state, which is not observed in experiment, one can only partially account for the influence of electronic correlations within the DFT-GGA framework. For  $\alpha$ -Fe we obtain a relatively small correction to GGA, which already reproduces the experimental values quite well.

In Fig 1b we compare the LDA+DMFT and GGA EOS with the one measured from Ref. [37]. Again, for both phases the LDA+DMFT approach successfully corrects the GGA overbinding error, which is relatively small in  $\alpha$ -Fe and very significant in  $\epsilon$ -Fe. Consequently, LDA+DMFT also reproduces correctly the volume change at the  $\alpha - \epsilon$  transition (about 5%), which is grossly overestimated in GGA. The  $c/a$  ratio in the hcp  $\epsilon$  phase is also affected by the electronic correlations. As shown in Fig 1c, the GGA calculations predict a reduction of the  $c/a$  ratio with increasing volume, from 1.59 at  $V=58$  a.u.<sup>3</sup>/atom to 1.58 at  $V=70$  a.u.<sup>3</sup>/atom. Within LDA+DMFT the  $c/a$  ratio remains almost constant and is close to the value of 1.60, in good agreement with ex-

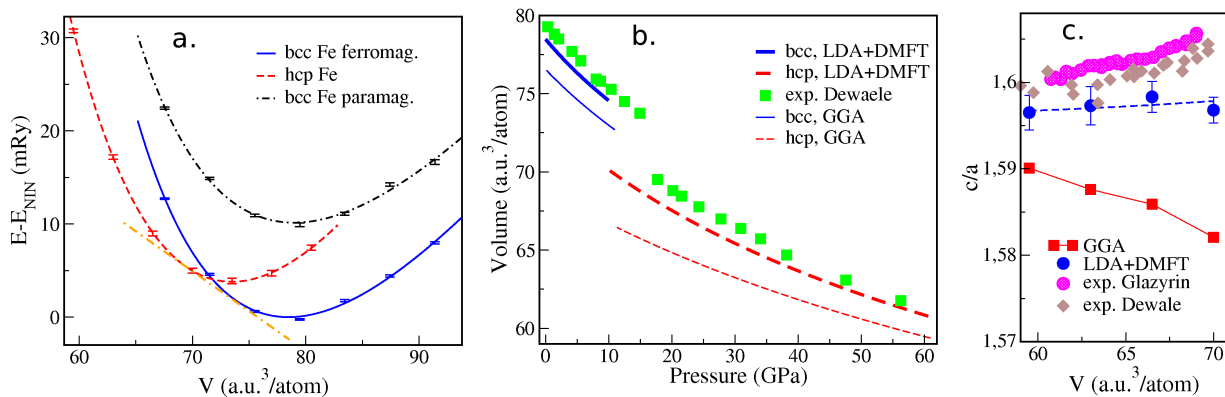


FIG. 1: (Color online). a). LDA+DMFT total energy vs. volume per atom for bcc (ferromagnetic, solid blue line, and paramagnetic, dot-dashed black line) and hcp (dashed red line) Fe. The error bars are the CT-QMC method stochastic error. The orange long dash-dotted straight line indicates the common tangent construction for the  $\alpha - \epsilon$  transition. b). Equations of states (EOS) for ferromagnetic bcc (low pressure) and paramagnetic hcp (high pressure) Fe. Theoretical results are obtained by fitting the LDA+DMFT (thick line) and GGA (thin line) total energies, respectively, using the Birch-Murnaghan EOS [36]. The experimental EOS of iron shown by green filled squares is from Dewaele et al., Ref. [37]. c). The ratio of lattice parameters  $c/a$  of  $\epsilon$ -Fe vs. volume per atom obtained in LDA+DMFT (blue circles, dashed line) and GGA (red squares, solid line). The experimental data are from Dewaele et al. [37] (diamonds) and Glazyrin et al. [21] (pink circles).

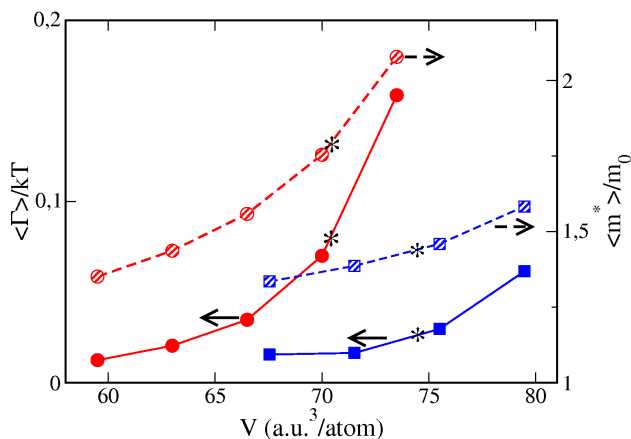


FIG. 2: (Color online) The ratio of the average inverse quasiparticle lifetime  $\langle \Gamma \rangle$  to temperature (the left axis) and the average mass enhancement  $\langle m^* \rangle / m_0$  (the right axis) vs. volume per atom. The solid lines (filled symbols) and dashed lines (hatched symbols) are  $\langle \Gamma \rangle / T$  and  $\langle m^* \rangle / m_0$ , respectively. The values for bcc and hcp phases are shown by blue squares and red circles, respectively. The black stars indicate the bcc and hcp atomic volumes at the transition point, respectively.

perimental measurements [47].

One may see that the ground-state properties (bulk modulus, equilibrium volume, etc.) of the  $\epsilon$  phase are significantly modified within the LDA+DMFT approach as compared to GGA. In contrast, for ferromagnetic  $\alpha$ -Fe those modifications are much weaker. In order to understand the origin of this difference we have evaluated the strength of the correlation ef-

fects in both phases from the low-frequency behavior of the local DMFT self-energy  $\Sigma(i\omega)$  on the Matsubara grid. Namely, we computed the average mass enhancement  $\langle m^* \rangle / m_0$  as  $\sum_s m_s^* N_s(E_F) / \sum_s N_s(E_F)$ , where the  $s$  index designates combined spin and orbital quantum numbers  $\{\sigma, m\}$ ,  $\Sigma_s(i\omega)$  and  $N_s(E_F)$  are the imaginary-frequency DMFT self-energy and partial density of states at the Fermi level for orbital  $s$ , respectively,  $m_s^* = 1 - [d\Im\Sigma_s(i\omega)/d\omega|_{\omega \rightarrow 0}]$  is the corresponding orbitally-resolved mass enhancement. We have also evaluated the average inverse quasiparticle lifetime  $\langle \Gamma \rangle = -\frac{m_0}{\langle m^* \rangle} \frac{\sum_s N_s(E_F) \Im\Sigma_s(\omega=0)}{\sum_s N_s(E_F)}$ . The resulting average mass enhancement and inverse quasiparticle lifetime are plotted in Fig. 2. In ferromagnetic  $\alpha$ -Fe both quantities slowly decay with decreasing volume and then they exhibit a large enhancement across the  $\alpha - \epsilon$  transition, indicating a more correlated nature of  $\epsilon$ -Fe. The latter is characterized by heavier quasiparticles, a larger electron-electron scattering and a stronger volume dependence of the correlation strength as compared to the bcc phase. This analysis clearly demonstrates that dynamical many-body effects are enhanced in the  $\epsilon$  phase.

Why are the electronic correlations in  $\epsilon$ -Fe stronger and why does the DFT fail there? The crucial difference is the magnetism. In  $\alpha$ -Fe, the physics is governed by the large static exchange splitting which easily polarizes the paramagnetic state characterized by a peak in the density of states (DOS) close to the Fermi energy. Therefore, the spin-polarized DFT-GGA calculations, which are able to capture this static exchange splitting, reproduce the ground state properties of ferromagnetic  $\alpha$ -Fe rather well. In antiferromagnetic  $\epsilon$ -Fe obtained within DFT-GGA the

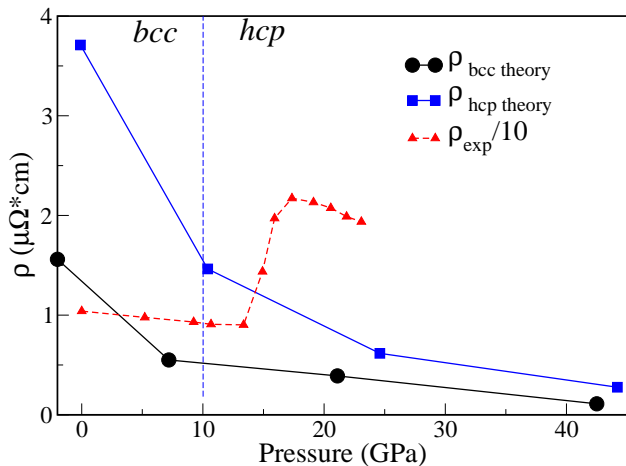


FIG. 3: (Color online) The electron-electron contribution to the resistivity in bcc  $\alpha$ -Fe (black circles, ) and hcp  $\epsilon$ -Fe (blue squares) computed within LDA+DMFT for  $T=294$  K. The experimental room-temperature resistivity [16] (red triangles, dashed line) is shown divided by 10. The vertical dot-dashed line indicate the theoretical transition pressure.

static exchange splitting also reduces the bonding leading to an improved agreement with the experimental equation of state. In contrast, dynamical many-body effects must be included to describe the experimental paramagnetic state of  $\epsilon$ -Fe properly. In this respect we note that the many-body corrections to the total energy and spectral properties were shown to be important [20, 38, 39] for the high-temperature nonmagnetic state of  $\alpha$ -Fe as well. If one suppresses magnetism,  $\alpha$ -Fe is actually even more correlated than  $\epsilon$ -Fe, which is a consequence of its large DOS close to the Fermi energy [40]. This larger DOS implies slower quasiparticles which are influenced by the interactions, especially the Hund's rule coupling [41].

We now turn to transport. The drop in the quasiparticle lifetime across the  $\alpha - \epsilon$  transition affects the electron-electron-scattering (EES) contribution to the resistivity  $\rho_{\text{el.-el.}}$ . We have calculated the evolution of the room-temperature  $\rho_{\text{el.-el.}}$  versus pressure in both phases, as displayed in Fig. 3. One may see that the behavior of  $\rho_{\text{el.-el.}}$  under pressure reflects that of the inverse quasiparticle lifetime  $\Gamma$ . The resistivity decays with pressure except at the transition point where a step-wise increase is found. A rapid enhancement of  $\rho_{\text{el.-el.}}$  in the  $\epsilon$  phase at pressures below  $P_c = 10$  GPa is in agreement with very recent measurements [42], in which a large hysteresis in the  $\alpha - \epsilon$  transition was obtained with the transition shifted to 7 GPa at the depressurization, and a very similar rapid increase in the total resistivity upon the decrease of pressure was observed in  $\epsilon$ -Fe for pressures below the usual experimental  $P_c$  of 12-15 GPa.

Now we discuss a very interesting point: despite the good qualitative agreement, the magnitude of the resis-

tivity enhancement through the transition to  $\epsilon$ -Fe in our calculations underestimates the values found in the experiment [16], by a factor of 10, see Fig. 3 [48]. The calculations of the electron-phonon-scattering (EPS) contribution to resistivity in Ref. [17] reproduce the resistivity of the bcc-Fe well but exhibit almost no change across the transition. Therefore, the corresponding jump of the measured total resistivity has to be attributed to electron-electron scattering. If the experimental issues, such as the sample thinning can be excluded, then the missing scattering that we find in comparison with experiments has to be associated with non-local long-range effects, which are not dealt with in our calculations. Interestingly, except for the magnitude, the pressure dependence of the resistivity is accounted well by our results. This might be understood by recognizing that the local correlations that suppress the coherence scale (the kinetic energy) also make the electronic degrees of freedom more prone to the effects of the coupling to the long-range spin-fluctuations.

It is interesting to compare  $\epsilon$ -Fe and  $\text{Sr}_2\text{RuO}_4$ , a widely investigated unconventional superconductor with similar transition temperature [43], to make a further link with spin fluctuations. Both materials display low-temperature unconventional superconductivity [43] and several mechanisms have been discussed to be at its origin [44]. In  $\text{Sr}_2\text{RuO}_4$  superconductivity emerges from a well-established Fermi liquid with  $T_{\text{FL}} = 25\text{K}$ . Local approaches, like the one used in this work, yield much shorter lifetimes [45] and a resistivity which agrees with experiments at low temperatures within 30%. [46] The picture is different for  $\epsilon$ -Fe, which displays a non-Fermi-liquid  $T^{5/3}$  temperature dependence of its low-temperature resistivity, [18] extending up to a temperature  $T^*$  which reaches the peak  $T_{\text{max}}^* \approx 35\text{K}$  at a pressure where superconductivity reaches its maximum [42]. Spin fluctuations, which are believed to be responsible for this behavior [15] have, hence, a very strong effect in  $\epsilon$ -Fe. Because their non-local nature cannot be captured within our framework, we believe that they are at the origin of the discrepancy between the experimental and our calculated resistivities.

In summary, including local correlations crucially improves the theoretical picture of  $\epsilon$ -Fe by correctly accounting for a set of experimental observations within the paramagnetic state. This solves the long-standing controversy between theory and experiment for this material. The successful description of Fe within the paramagnetic state, together with an underestimation of the resistivity found in our local approach, hints at the importance of spin fluctuations, which supports scenarios relating them to the origin of superconductivity.

Acknowledgment: We are grateful to A. Georges and D. Jaccard for useful discussions. The input of X. Deng in the development of the transport code is gratefully acknowledged. L. P. acknowledges the travel support

provided by PHD DALEN Project 26228RM. J. M. acknowledges the support of College de France where a part of this work was done and the Slovenian research agency program P1-0044. O. P. acknowledges support by ERC under grant 278472 - MottMetals. The computations were performed on resources provided by the Swedish National Infrastructure for Computing (SNIC) at the National Supercomputer Centre(NSC) and PDC Center for High Performance Computing.

- 
- [1] S. Tatenò, K. Hirose, Y. Ohishi, and Y. Tatsumi, *Science* **330**, 359 (2010).
- [2] O. Mathon, F. Baudelet, J. P. Itié, A. Polian, M. d’Astuto, J. C. Chervin, and S. Pascarelli, *Phys. Rev. Lett.* **93**, 255503 (2004).
- [3] A. Monza, A. Meffre, F. Baudelet, J.-P. Rueff, M. d’Astuto, P. Munsch, S. Huotari, S. Lachaize, B. Chaudret, and A. Shukla, *Phys. Rev. Lett.* **106**, 247201 (2011).
- [4] D. Bancroft, E. L. Peterson, and S. Minshall, *Journal of Applied Physics* **27**, 291 (1956).
- [5] K. Shimizu, T. Kimura, S. Furomoto, K. Takeda, K. Kontani, Y. Onuki, and K. Amaya, *nat* **412**, 316 (2000).
- [6] P. Pedrizzini, D. Jaccard, G. Lapertot, J. Flouquet, Y. Inada, H. Kohara, and Y. Onuki, *Physica B: Condensed Matter* **378380**, 165 (2006).
- [7] G. Steinle-Neumann, L. Stixrude, and R. E. Cohen, *Phys. Rev. B* **60**, 791 (1999).
- [8] G. Steinle-Neumann, R. E. Cohen, and L. Stixrude, *Journal of Physics: Condensed Matter* **16**, S1109 (2004).
- [9] M. Friák and M. Šob, *Phys. Rev. B* **77**, 174117 (2008).
- [10] R. Lizárraga, L. Nordström, O. Eriksson, and J. Wills, *Phys. Rev. B* **78**, 064410 (2008).
- [11] S. Merkel, A. F. Goncharov, H.-k. Mao, P. Gillet, and R. J. Hemley, *Science* **288**, 1626 (2000).
- [12] G. Steinle-Neumann, L. Stixrude, and R. E. Cohen, *Proceedings of the National Academy of Sciences* **101**, 33 (2004).
- [13] G. Cort, R. D. Taylor, and J. O. Willis, *Journal of Applied Physics* **53**, 2064 (1982).
- [14] A. B. Papandrew, M. S. Lucas, R. Stevens, I. Halevy, B. Fultz, M. Y. Hu, P. Chow, R. E. Cohen, and M. Somayazulu, *Phys. Rev. Lett.* **97**, 087202 (2006).
- [15] I. I. Mazin, D. A. Papaconstantopoulos, and M. J. Mehl, *Phys. Rev. B* **65**, 100511 (2002).
- [16] A. T. Holmes, D. Jaccard, G. Behr, Y. Inada, and Y. Onuki, *Journal of Physics: Condensed Matter* **16**, S1121 (2004).
- [17] X. Sha and R. E. Cohen, *Journal of Physics: Condensed Matter* **23**, 075401 (2011).
- [18] D. Jaccard and A. T. Holmes, *Physica B: Condensed Matter* **359361**, 333 (2005).
- [19] A. I. Lichtenstein, M. I. Katsnelson, and G. Kotliar, *Phys. Rev. Lett.* **87**, 067205 (2001).
- [20] I. Leonov, A. I. Poteryaev, V. I. Anisimov, and D. Vollhardt, *Phys. Rev. Lett.* **106**, 106405 (2011).
- [21] K. Glazyrin, L. V. Pourovskii, L. Dubrovinsky, O. Narygina, C. McCammon, B. Hewener, V. Schünemann, J. Wolny, K. Muffler, A. I. Chumakov, et al., *Phys. Rev. Lett.* **110**, 117206 (2013).
- [22] M. Aichhorn, L. Pourovskii, V. Vildosola, M. Ferrero, O. Parcollet, T. Miyake, A. Georges, and S. Biermann, *Phys. Rev. B* **80**, 085101 (2009).
- [23] M. Aichhorn, L. Pourovskii, and A. Georges, *Phys. Rev. B* **84**, 054529 (2011).
- [24] P. Blaha, K. Schwarz, G. Madsen, D. Kvasnicka, and J. Luitz, *WIEN2k, An augmented Plane Wave + Local Orbitals Program for Calculating Crystal Properties* (Techn. Universitat Wien, Austria, ISBN 3-9501031-1-2., 2001).
- [25] A. Georges, G. Kotliar, W. Krauth, and M. J. Rozenberg, *Rev. Mod. Phys.* **68**, 13 (1996).
- [26] E. Gull, A. J. Millis, A. I. Lichtenstein, A. N. Rubtsov, M. Troyer, and P. Werner, *Rev. Mod. Phys.* **83**, 349 (2011).
- [27] M. Ferrero and O. Parcollet, "TRIQS: a Toolbox for Research on Interacting Quantum Systems", <http://ipht.cea.fr/triqs>.
- [28] T. Miyake, F. Aryasetiawan, and M. Imada, *Phys. Rev. B* **80**, 155134 (2009).
- [29] M. Casula, P. Werner, L. Vaugier, F. Aryasetiawan, T. Miyake, A. J. Millis, and S. Biermann, *Phys. Rev. Lett.* **109**, 126408 (2012).
- [30] M. T. Czyżyk and G. A. Sawatzky, *Phys. Rev. B* **49**, 14211 (1994).
- [31] A. E. Antipov, I. S. Krivenko, V. I. Anisimov, A. I. Lichtenstein, and A. N. Rubtsov, *Phys. Rev. B* **86**, 155107 (2012).
- [32] V. S. Oudovenko, G. Pálsson, K. Haule, G. Kotliar, and S. Y. Savrasov, *Phys. Rev. B* **73**, 035120 (2006).
- [33] C. Ambrosch-Draxl and J. O. Sofo, *Computer Physics Communications* **175**, 1 (2006).
- [34] H. C. Herper, E. Hoffmann, and P. Entel, *Phys. Rev. B* **60**, 3839 (1999).
- [35] H. K. Mao, Y. Wu, L. C. Chen, J. F. Shu, and A. P. Jephcoat, *Journal of Geophysical Research: Solid Earth* **95**, 21737 (1990).
- [36] F. Birch, *Phys. Rev.* **71**, 809 (1947).
- [37] A. Dewaele, P. Loubeyre, F. Occelli, M. Mezouar, P. I. Dorogokupets, and M. Torrent, *Phys. Rev. Lett.* **97**, 215504 (2006).
- [38] A. A. Katanin, A. I. Poteryaev, A. V. Efremov, A. O. Shorikov, S. L. Skornyakov, M. A. Korotin, and V. I. Anisimov, *Phys. Rev. B* **81**, 045117 (2010).
- [39] L. V. Pourovskii, T. Miyake, S. I. Simak, A. V. Ruban, L. Dubrovinsky, and I. A. Abrikosov, *Phys. Rev. B* **87**, 115130 (2013).
- [40] R. Maglic, *Phys. Rev. Lett.* **31**, 546 (1973).
- [41] A. Georges, L. de’Medici, and J. Mravlje, *Annu. Rev. Cond. Matt. Phys.* **4**, 137 (2013).
- [42] C. S. Yadav, G. Seyfarth, P. Pedrizzini, H. Wilhelm, R. Černý, and D. Jaccard, *Phys. Rev. B* **88**, 054110 (2013).
- [43] A. P. Mackenzie and Y. Maeno, *Rev. Mod. Phys.* **75**, 657 (2003).
- [44] Y. Maeno, S. Kittaka, T. Nomura, S. Yonezawa, and K. Ishida, *Journal of the Physical Society of Japan* **81**, 011009 (2012).
- [45] J. Mravlje, M. Aichhorn, T. Miyake, K. Haule, G. Kotliar, and A. Georges, *Phys. Rev. Lett.* **106**, 096401 (2011).
- [46] J. Mravlje, (unpublished).
- [47] The peculiarity in the  $c/a$  ratio in  $\epsilon$ -Fe discussed in

Ref. [21] cannot be resolved in our calculations. It is an order of magnitude smaller than the error bars due to CT-QMC stochastic error

[48] Note that plot 2 suggests quite long scattering life-

times. The transport scattering time  $\tau_{\text{tr}}$  is an average of  $-1/[2\Im\Sigma(\omega)]$  over the window opened by the Fermi function. For  $\epsilon$ -Fe at  $T=295$  K one obtains  $\tau_{\text{tr}} \approx 80$ fs.